

Research article

# Acoustic emission analysis and signal classification for damage modes in UD carbon/epoxy composites

Gergő Zsolt Marton<sup>1,2</sup>, Fanni Balogh<sup>1,2</sup>, Gábor Szabó<sup>1,2\*</sup>

<sup>1</sup>Department of Polymer Engineering, Faculty of Mechanical Engineering, Budapest University of Technology and Economics, Műegyetem rkp. 3., H-1111 Budapest, Hungary

<sup>2</sup>MTA-BME Lendület Sustainable Polymers Research Group, Műegyetem rkp. 3., H-1111 Budapest, Hungary

Received 13 May 2025; accepted in revised form 2 June 2025

**Abstract.** The failure of fiber-reinforced polymer composites is considered a complex process resulting from several concurrent damage mechanisms and their interactions. To better understand the damage modes of composites, which is necessary to ensure their structural health monitoring, increase their reliability, and validate different methods used for influencing their damage and failure process, it is crucial to detect, identify, and analyze different damage modes present in composite materials. The acoustic emission technique provides the opportunity to acquire damage-related data, which can be analyzed and associated with different modes of damage. In the current study, we conducted specific tests using the acoustic emission (AE) technique on the composite and its constituents, which can induce individual damage modes, thereby enabling the determination of their characteristic AE signal properties and their identification in complex composite structures.

**Keywords:** composite, damage, failure, acoustic emission, damage analysis

## 1. Introduction

Composite materials have gained importance in several industries over the past decades, particularly in the automotive and aerospace sectors, mainly due to their low density and outstanding mechanical properties. However, their structural complexity makes them prone to sudden, catastrophic failure, which might be disadvantageous in areas with high quality requirements [1–3]. Therefore, there is a growing demand for composite materials that can reach the end of their service life in a predetermined way, thereby making their use safer and more predictable. Different methods exist where the initiation – *e.g.*, by artificial damage – or the propagation of damage, or even both – designed failure – can be determined in advance [4–9].

However, before influencing the damage process of composite materials, we need to understand their

damage processes and failure modes clearly. Damage on different levels is always present in composite materials and can be derived from various sources, such as defects in raw materials, damage induced by the manufacturing process, or in-service. Besides, damage in composites can vary significantly in size and impact on the structural integrity as well. Damage initiation, propagation, and mode of macroscopic failure depend primarily on the loading conditions. The failure of composites can be described as the result of several different concurring and interfering damage mechanisms working simultaneously. On the macroscopic level, four basic modes of damage can lead to the failure of the composite structure: fibre fracture, fibre-matrix debonding, matrix cracking, delamination [10–13].

Detection of damage in composite materials is critical to ensure proper structural health monitoring,

\*Corresponding author, e-mail: [szabenyi@pt.bme.hu](mailto:szabenyi@pt.bme.hu)

© BME-PT

thereby maintaining the structural integrity of composites. Furthermore, it is inevitable to accurately identify and analyze the different damage processes occurring in the material and the failure mode's characteristics to improve composites' reliability and in-service behavior [14–16].

Damage analysis often proves to be challenging. However, non-destructive testing (NDT) methods can be used for this purpose. There are several methods with various benefits and limitations – *e.g.*, in terms of detectable damage type and size – in the NDT testing of composite materials. When selecting the appropriate NDT method, it is essential to consider the advantages and disadvantages of each technique, or combining at least two methods to mitigate their limitations might also be favorable. Methods such as ultrasonic testing, digital image correlation (DIC), infrared thermography (IRT), and computed tomography (CT) are often used for the investigation of composites [15, 17–23].

The acoustic emission (AE) technique, which is based on the detection and analysis of acoustic waves generated by the energy emitted by active damage mechanisms, is a common method in the field of composite materials as well. Besides damage detection, the AE technique enables the localization of damage initiation and propagation based on the time difference of signal arrival and the identification and monitoring of different damage mechanisms by analyzing different signal properties such as amplitude, frequency, signal strength, etc. A typical AE signal with the definition of the signal properties can be seen in Figure 1 [24–30].

Analyzing these parameters can contribute to identifying different damage mechanisms and provide

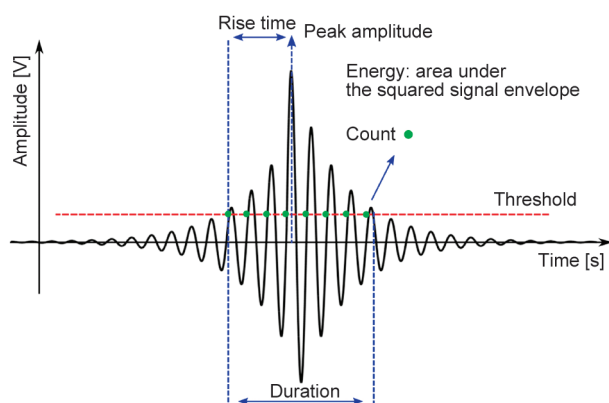


**Figure 1.** Interpretation of acoustic emission signal properties [24] (figure licensed under the Creative Commons Attribution 4.0 International License (CC BY 4.0)).

insights into the material's structural integrity. Amplitude, measured in dB, means the peak voltage of the signal and can be considered a key parameter of the acoustic emission technique. Based on related studies, more significant damage mechanisms can be associated with signals with a higher amplitude. The active damage mechanism, which is the source of the AE signal, might be well characterized by the absolute energy of the signal. Besides amplitude and energy analysis, signal strength, which is related to the total power of the AE signal, can give additional information on the severity of damage. Research studies show that the frequency of the signal may be extremely useful in identifying individual damage mechanisms. Counts mean the number of threshold crossings; thereby, this property can be connected to the complexity of the acoustic event. Besides, rise time, which is equal to the time between the first threshold crossing and the peak amplitude, can characterize the temporal evolution of the signal [24, 31, 32].

Experimental studies underline the importance of designing controlled tests that isolate individual damage mechanisms to build accurate AE signal databases. However, it should be noted that the analysis of AE signals in relevant research is typically based on only one or two key properties – most commonly amplitude and peak frequency. Furthermore, it is essential that the characteristic AE signal ranges associated with specific damage mechanisms can vary significantly depending on the type of reinforcement or matrix material used. Furthermore, the classification of AE signals may be carried out manually or using clustering methods and signal processing. The application of machine learning techniques can also be helpful, *e.g.*, creating artificial neural networks (ANN) offers promising results for damage analysis [24, 33–39].

NDT methods, primarily acoustic emission, may provide the opportunity to develop appropriate test systems to assess different damage modes. To achieve this, we carried out different tests, providing damage processes, predominantly present in composites, supported by AE measurements, which allowed us to analyze and characterize various types of damage separately.

The main goal of the current research was to investigate in detail the main damage modes of carbon fiber/epoxy composite materials, to determine their characteristic AE properties, and to develop a comprehensive evaluation system for damage assessment.

The developed system may provide a more accurate picture of the various damage processes by connecting a physical meaning derived from the different tests, inducing individual damage modes to their classification based on AE properties. The determination of the characteristic signal properties can also support statistical clustering methods *e.g.* in terms of pre-processing data, specifying the parameters of the clustering method and associating clusters with damage modes. The obtained results provide additional information related to the primary damage mechanisms of composite materials and may contribute to their safer and more reliable application, as well as promote the development of their structural health monitoring methods.

## 2. Materials and methods

### 2.1. Materials

Panex35 (Zoltek Zrt., Nyergesújfalu, Hungary) 50k rovings were used for tensile tests both dry and after resin-impregnation. Individual fibers for the microbond tests and the single fiber tensile tests were taken from the same type of roving. As reinforcement material of the manufactured composites, we used PX35FBUD0300 (Zoltek Zrt., Nyergesújfalu, Hungary) stitch-bonded unidirectional carbon weave (309 g/m<sup>2</sup> surface weight), consisting of Panex35 50k rovings. IPOX MR 3010 (IPOX Chemicals Kft., Budapest, Hungary) DGEBA-based epoxy resin (EP) mixed with IPOX MH 3124 amine type curing agent in a weight ratio of 100:35 was used for the manufacturing of specimens for epoxy tensile tests and as matrix material for microbond tests, tensile tests of impregnated rovings and short-beam shear tests.

### 2.2. Sample production

Epoxy specimens for tensile testing were cast in silicon molds, following the 1A geometry of the ISO 527-2 standard. For the single fiber tensile and microbond tests, carbon fibers were extracted from rovings and mounted on a paper frame to ensure a consistent gauge length of 25 mm. In the case of the microbond tests, a microdroplet of epoxy resin was deposited onto each individual fiber to enable the evaluation of the fiber–matrix interfacial strength. For the tensile testing of dry and impregnated rovings, specimens with a length of 250 mm were prepared. Bonded composite end-tabs were applied to protect the specimens from the grips during tensile tests, resulting in a free length of 150 mm.

Composite plates with a [0<sub>6</sub>] layup configuration were fabricated using vacuum infusion resulting in a nominal thickness of 2.5 mm. For the short-beam shear (SBS) tests, specimens were cut from the plates following the ISO 14130 standard, using a Mutronic Diadisc (Mutronic, Rieden am Forggensee, Germany) diamond disc cutter.

### 2.3. Methods

The acoustic emission testing was carried out with a Mistras PCI-2 (MISTRAS Group, Princeton Junction, USA) AE system. We used an IL40S preamplifier (Physical Acoustic Corporation, Princeton Junction, USA) with a gain of 40 dB and Micros30s (Physical Acoustic Corporation, Princeton Junction, USA) microphones (operating frequency range: 150–400 kHz). The measurement threshold was set to 30 dB. All AE sensors were coupled to the specimens or testing devices using Oxett (T-silox Ltd., Budapest, Hungary) silicon grease to ensure optimal signal transmission. AE data was processed with NOESIS 9.0 and MATLAB R2024b software. We conducted the single fiber tensile tests on a Zwick Z005 (Zwick GmbH, Ulm, Germany) universal testing machine equipped with a 20 N load cell and operated at a 2 mm/min crosshead speed. During the test, we applied an AE microphone directly to the fiber using silicon grease as coupling agent. The gauge length between the grips was set to 25 mm. In the case of single fibre tensile tests, 50 specimens were investigated. [Figure 2](#) demonstrates the experimental setup.

For the microbond tests, we employed the same Zwick Z005 universal testing machine with a 0.5 mm/min test speed. A dedicated micro bond device was fixed on the testing machine, incorporating two steel blades to support the resin droplet during the fiber-matrix debonding process. We adjusted the blade distance according to the diameter of the droplet, measured via an Olympus BX51M (Olympus Corporation, Tokyo, Japan) optical microscope, setting the blade spacing to approximately one-third of the droplet diameter. The AE microphone was mounted on an extension plate of one of the blades using silicon grease as coupling agent. The experimental setup is shown in [Figure 3](#). In case of microbond tests, 50 specimens were tested as well.

The tensile testing of epoxy specimens was carried out according to the ISO 527-2 standard at a crosshead speed of 5 mm/s using a Zwick Z005 (Zwick GmbH, Ulm, Germany) universal testing machine

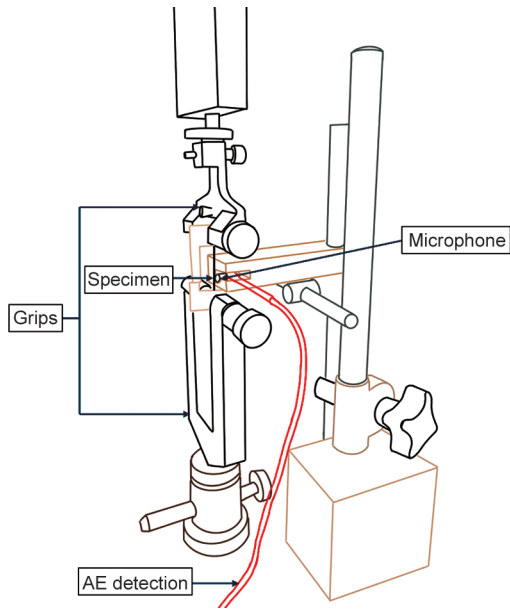


**Figure 2.** Experimental setup of a single fiber tensile test.

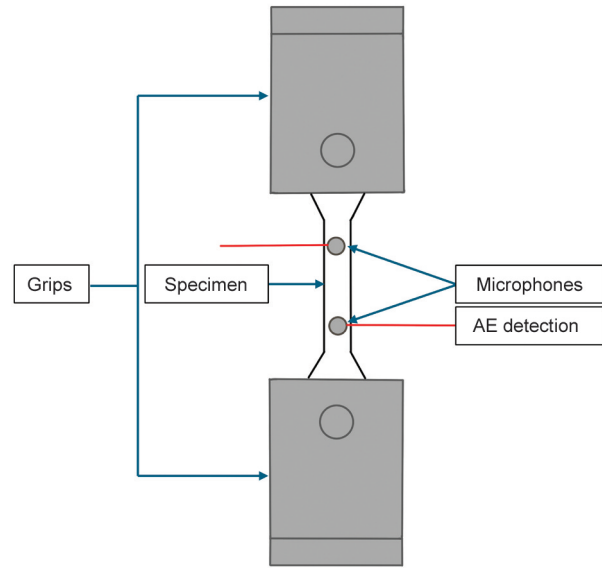


**Figure 4.** Experimental setup of a tensile test on an epoxy sample.

with a 5 kN load cell. We attached two AE microphones to each specimen with a spacing of 60 mm, using silicon grease as coupling agent. **Figure 4** shows the test setup of the epoxy tensile tests.

In case of the tensile testing of rovings in dry and impregnated form, 5–5 specimens. The tensile tests were done with a crosshead speed of 5 mm/s using a Zwick Z005 (Zwick GmbH, Ulm, Germany) universal testing machine with a 5 kN load cell. Two AE microphones were used with silicon grease as coupling agent to acquire signals with a sensor distance of 100 mm. The experimental setup can be seen in **Figure 5**.

We performed the short-beam shear (SBS) tests on 20 specimens following the ISO 14130 standard with a Zwick Z020 (Zwick GmbH, Ulm, Germany) universal testing machine equipped with a 20 kN

load cell. Although the standard specifies the loading head diameter, we employed a larger diameter loading cylinder to improve load distribution and minimize the possibility of local failure. The span length was 12.5 mm, and the test speed was 5 mm/min. During the SBS tests, the AE microphone's placement was considered when determining the specimen length, resulting in an asymmetric setup. One AE microphone was applied to each specimen using silicon grease as a coupling agent. **Figure 6** shows the experimental setup.

### 3. Results and discussion

To identify the characteristic features of AE signals corresponding to various failure modes, we analyzed six key signal parameters: rise time, count, amplitude,

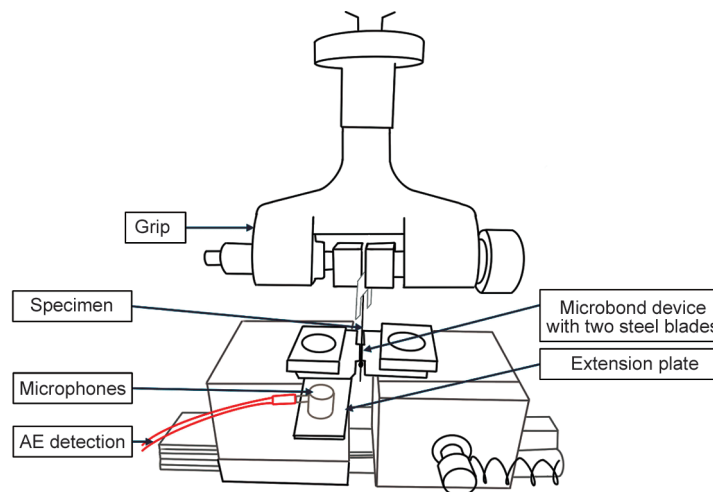


**Figure 3.** Experimental setup of a microbond test.

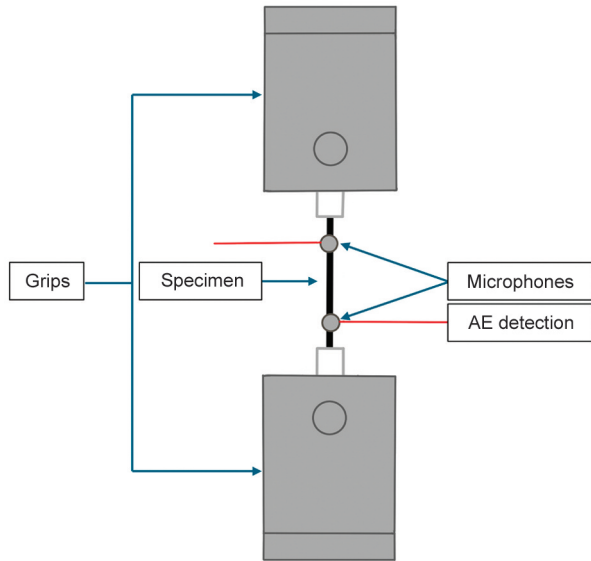


Figure 5. Experimental setup of tensile tests carried out on dry and impregnated rovings.

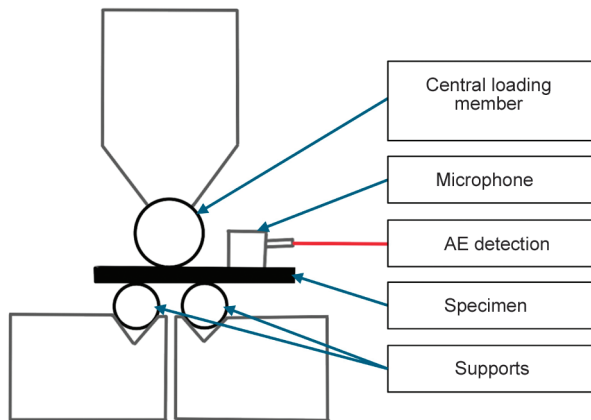


Figure 6. Experimental setup of a short-beam shear test.

average frequency, signal strength, and absolute energy. To eliminate non-damage-related noise, we excluded signals with amplitudes below 40 dB from the analysis, based on preliminary tests which indicated that crosshead motion and frictional effects could generate signals exceeding the 30 dB threshold.

The distributions of the selected AE parameters were analyzed to characterize the different damage modes.

To determine the representative value ranges for each failure mode, we calculated several percentile intervals (Q10\_Q90, Q15\_Q85, Q25\_Q75), allowing us to define the threshold values encompassing the central 50–80% of the data. These percentile ranges provide insight into signal characteristics' variability and typical range and are summarized in tabulated form. Besides, we used the Q2\_Q98 range for delamination, because it is a more complex damage mechanism, where strong interactions with other

damage mechanisms, such as matrix cracking and fiber-matrix debonding, can be observed.

### 3.1. Tensile testing of epoxy

From the AE data acquired during the tensile testing of epoxy specimens, we determined the properties of AE signals characteristic of matrix cracking. A typical tensile curve of an epoxy specimen and the amplitude of acoustic signals collected during the test are shown in Figure 7. Each tensile specimen demonstrated a brittle failure, demonstrating a tensile strength of  $35.0 \pm 3.5$  MPa. However, initiation and propagation of small matrix cracks, which may have been related to manufacturing-induced defects, e.g., voids in the material, were experienced during the tests. The results show that AE signals emitted by the damage processes occurring in the epoxy specimen can be related to the matrix cracking of a composite with the same epoxy matrix material. Besides, high-amplitude signals and their echoes can be detected directly at the global failure of the specimen.

The characteristic interval can be specified for each investigated signal property by analyzing the distribution of the different AE signal properties, shown in Table 1.

### 3.2. Microbond tests

Microbond tests measure interfacial shear strength by inducing debonding along the fiber-matrix interface. The tests carried out demonstrated an average interfacial shear strength of  $34.2 \pm 2.7$  MPa. A typical curve of a microbond test and the amplitude of the recorded AE signals is shown in Figure 8. For each test, two AE signals with at least 40 dB amplitude were recorded, which were followed in several cases by signals below 40 dB. As Figure 3 demonstrates, the first hit with higher amplitude occurs at the maximal force and can be explained by the start of the debonding process. Meanwhile, the second hit with

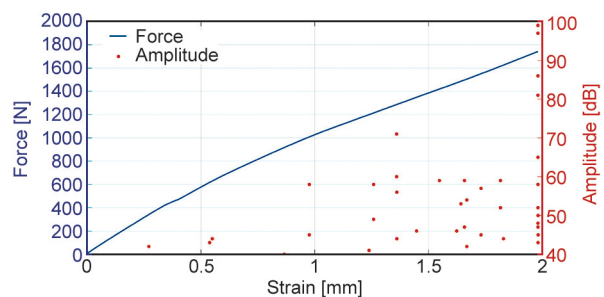
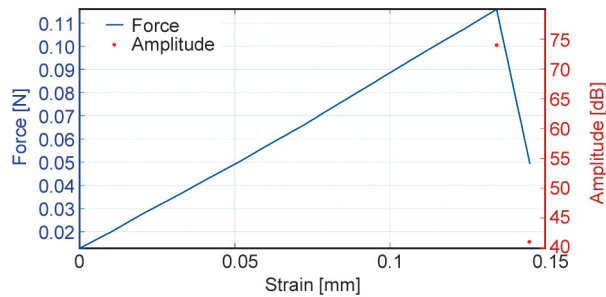


Figure 7. Typical tensile curve and AE data of an epoxy specimen.

**Table 1.** Characteristic signal properties of matrix cracking determined by epoxy tensile tests.

Parameter		Q10_Q90	Q15_Q85	Q25_Q75
Rise time	[ $\mu$ s]	4–51	5–41	6–24
Counts	[–]	7–38	8–31	9–25
Amplitude	[dB]	41–59	41–58	42–53
Average frequency	[kHz]	108–214	115–200	122–182
Signal strength	[pV·s]	1421–23 520	1699–17 068	2159–11 157
Absolute energy	[aJ]	8–702	10–408	15–180



**Figure 8.** Typical curve and AE data of a microbond test.

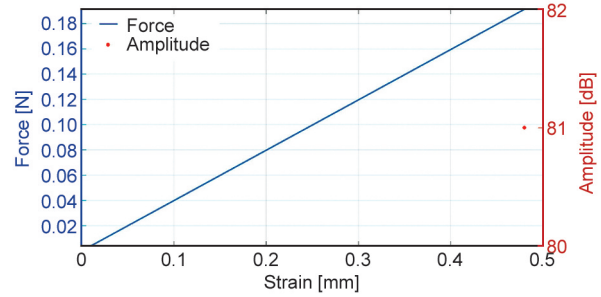


**Figure 9.** Typical tensile curve and AE data of a single fiber tensile test.

lower amplitude levels can be associated with friction between the fiber and the matrix droplet.

Analyzing the distribution of the signal properties, only the first signals with higher amplitude were considered for each test. This can be explained by the fact that only these signals can be related to fibre-matrix debonding as a damage mode itself. The determined characteristic intervals of the AE signal properties are shown in Table 2.

### 3.3. Single fiber tensile tests

Tensile tests with a single fiber can provide information about the characteristic AE signal properties for

fiber breakage. The investigated carbon fibers demonstrated an average tensile strength of  $4.7 \pm 0.2$  GPa. Figure 9 shows that a single fiber tensile test results in one high-amplitude AE hit acquired at the breaking force.

Table 3 shows the characteristic intervals of the AE signal properties related to fiber breakage determined by single fiber tensile tests.

### 3.4. Roving tensile tests

Tensile testing of rovings, compared to tests carried out with single fibers, can give a better understanding

**Table 2.** Characteristic signal properties of fiber-matrix debonding determined by microbond tests.

Parameter		Q10_Q90	Q15_Q85	Q25_Q75
Rise time	[ $\mu$ s]	22–59	23–52	26–39
Counts	[–]	141–205	147–202	160–190
Amplitude	[dB]	72–88	72–87	74–86
Average frequency	[kHz]	149–205	155–202	162–190
Signal strength	[pV·s]	240 330–1 047 557	298 464–955 619	412 739–864 073
Absolute energy	[aJ]	35 063–784 609	44 849–740 601	64 879–387 511

**Table 3.** Characteristic signal properties of fiber breakage determined by single fiber tensile tests.

Parameter		Q10_Q90	Q15_Q85	Q25_Q75
Rise time	[ $\mu$ s]	7–58	7–53	8–38
Counts	[–]	81–168	85–166	90–154
Amplitude	[dB]	71–91	72–89	76–85
Average frequency	[kHz]	148–294	156–268	167–259
Signal strength	[pV·s]	93 592–943 014	109 852–890 457	157 861–766 021
Absolute energy	[aJ]	14 095–692 027	15 126–512 761	30 738–29 5046

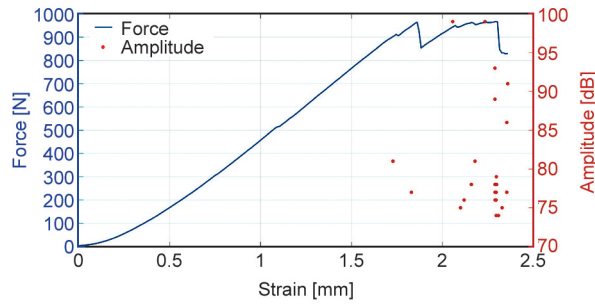


**Figure 10.** Typical tensile curve and AE data of a roving tensile test.

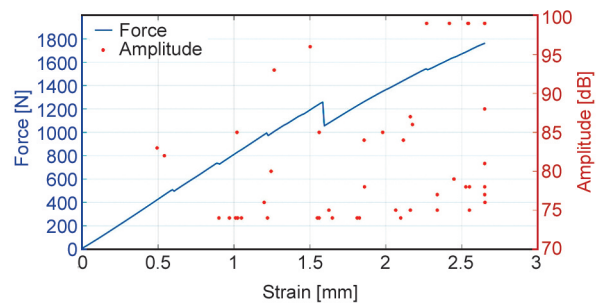


**Figure 11.** Typical tensile curve and AE data of an impregnated roving tensile test.

of fiber breakage as a damage process in composite materials, which is often built up as the sequence of the failure of several fibers inside the same roving. The investigated rovings failed at an average force of  $940.7 \pm 40.8$  N. As Figure 10 demonstrates, first, the weakest fibers fail, resulting in few signals with amplitudes between 75–85 dB. Reaching the maximum force, more fibers fail, resulting in AE signals with amplitudes up to 100 dB.

Table 4 shows the characteristic intervals of the AE signal properties related to fiber breakage specified by roving tensile tests.

### 3.5. Impregnated roving tensile tests

In a composite structure, the fibers are impregnated with matrix material, where the matrix is responsible for load transfer between fibers. The matrix can modify the sequential failure of several fibers and fiber bundles compared to a dry rovings. The impregnation of the reinforcement fibers by matrix material may influence the energy emitted by the active

damage mechanism, thereby affecting the acquired acoustic wave and its properties. Therefore, tensile testing of impregnated rovings might provide more similar signals to real-life composite structures and additional information on the manner and complexity of fiber breakage as a damage mode of fiber-reinforced polymer composites. The investigated specimens failed at an average force of  $1841.1 \pm 76.2$  N. It should be noted that in the case of tensile testing of impregnated rovings, a complex damage mechanism is investigated. In addition to fiber breakage, fiber-matrix debonding and matrix fracture are also present. Figure 11 shows a typical tensile curve and the amplitude of AE hits after filtering out the signals associated with the matrix fracture based on the signal properties determined by tensile testing of epoxy. This means that the accepted signals are related to fiber breakage or fiber-matrix debonding.

Table 5 contains the characteristic intervals of the AE signal properties acquired during impregnated roving tensile tests.

**Table 4.** Characteristic signal properties of fiber breakage determined by roving tensile tests.

Parameter		Q10_Q90	Q15_Q85	Q25_Q75
Rise time	[ $\mu$ s]	84–935	171–871	293–850
Counts	[–]	197–280	213–272	230–263
Amplitude	[dB]	75–92	76–89	76–81
Average frequency	[kHz]	197–280	213–272	230–263
Signal strength	[pV·s]	333 873–1 652 293	371 011–1 257 353	413 842–909 086
Absolute energy	[aJ]	41 403–1 876 683	43 852–602 452	60 727–228 336

**Table 5.** Characteristic signal properties of AE signals recorded during impregnated roving tensile tests.

Parameter		Q10_Q90	Q15_Q85	Q25_Q75
Rise time	[ $\mu$ s]	109–858	119–740	214–607
Counts	[–]	227–298	232–297	238–295
Amplitude	[dB]	74–99	74–99	74–86
Average frequency	[kHz]	227–298	232–297	238–295
Signal strength	[pV·s]	431 108–5 473 814	523 308–2 895 760	572 631–1 292 062
Absolute energy	[aJ]	72 889–20 598 142	82 660–10 951 284	99 958–619 386

### 3.6. Short-beam shear tests

A short-beam shear test is helpful in investigating the interlaminar properties of polymer composites by inducing high interlaminar shear stresses, resulting in delamination as the primary mode of damage and failure. Therefore, carrying out short-beam shear tests supported by the AE technique enables the detection of mainly delamination-related AE hits. However, other damage modes may be present, such as matrix cracking and fiber-matrix debonding. Figure 12 shows a typical curve of a short-beam shear test with the related AE data after filtering out signals associated with matrix cracking and fiber-matrix debonding

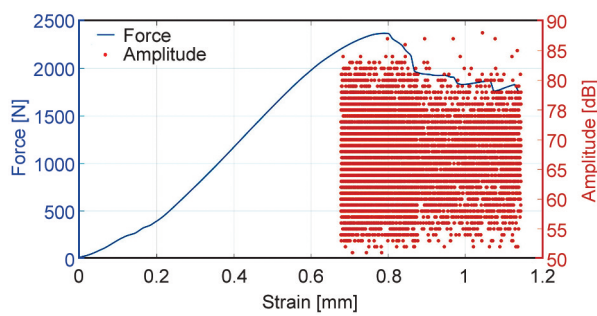


Figure 12. Typical curve and AE data of a short-beam shear test.

based on the characteristic intervals specified by tensile testing of epoxy and microbond tests.

Table 6 summarizes the characteristic intervals of the AE signal properties associated with delamination.

### 3.7. Classification of signals

The results of the conducted tests can be used to identify damage modes and to specify the properties that make it possible to differentiate between them. The data used for this purpose is shown in Figures 13-18. The boxplots highlight the distribution and variability of AE signal properties across damage modes.

In terms of amplitude (Figure 13), a parameter closely related to the intensity of the signal, matrix cracking consistently exhibits the lowest amplitudes, typically below 60 dB, followed by delamination with amplitudes mainly between 60–70 dB. Other, fiber or interface-related damage mechanisms reach higher peak amplitudes. An overlap can be observed between debonding and fiber breakage. However, investigating data acquired from impregnated roving testing can help distinguish between them.

The results of the impregnated roving tensile tests (‘complex damage’) must include signals related to

Table 6. Characteristic signal properties of delamination determined by short-beam shear tests.

Parameter		Q10_Q90	Q15_Q85	Q25_Q75	Q2_Q98
Rise time	[ $\mu$ s]	68–896	114–841	207–732	7–987
Counts	[–]	161–208	169–205	178–201	97–216
Amplitude	[dB]	57–74	58–72	60–70	54–79
Average frequency	[kHz]	165–208	171–205	179–201	147–216
Signal strength	[pV·s]	64 550–270 020	70 319–236 529	82 387–187 888	46 434–377 841
Absolute energy	[aJ]	1170–36 072	1405–26 133	2021–15 138	851–86 555

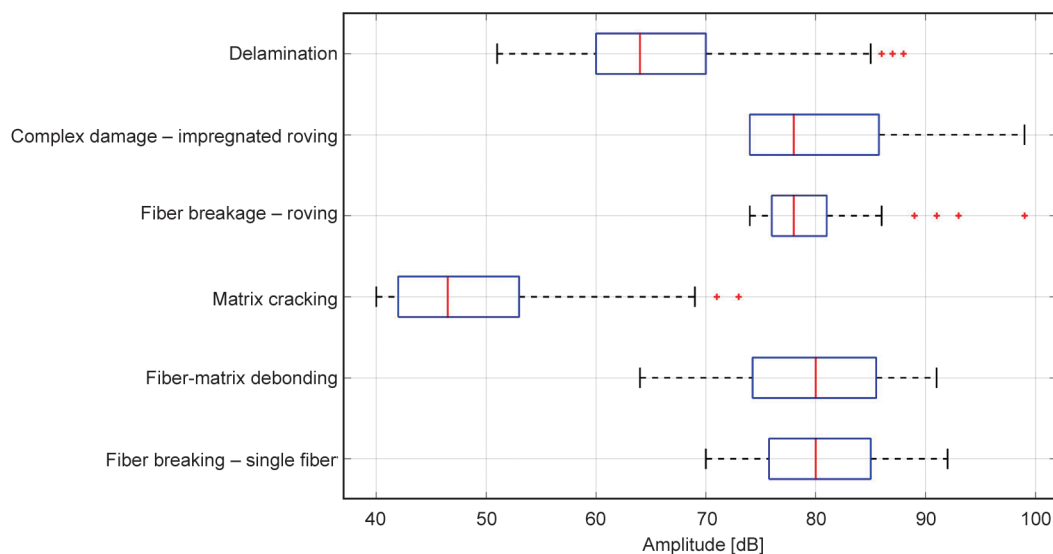


Figure 13. Amplitude distribution of various damage modes represented by horizontal box plots.

two damage modes: fiber breakage and fiber-matrix debonding. However, comparing the signal properties indicates that the lower amplitude signals – around 75 dB – of the impregnated roving tensile tests (Figure 11) are significantly more similar in their properties to the signals detected during the microbond test, which suggests that these signals may originate predominantly from fiber–matrix debonding. In contrast, higher amplitude signals – above 80 dB – might be associated with fiber breakage. This can be supported by the fact that these signals are more similar to the AE signal acquired during the roving tensile tests.

When examining counts (Figure 14), matrix cracking holds the lowest values, generally under 50 counts. Such low values suggest that this failure mode generates less complex AE events. Meanwhile, other damage mechanisms can be associated with significantly higher counts. Fiber breakage in rovings and complex damage in impregnated rovings demonstrate the highest values, often exceeding 200. The results of the impregnated roving tests indicate that their damage processes are more dominated by fiber breakage. Besides, it should be noted that roving testing may provide a better characterization of fiber breakage within the composite than individual fiber testing. Furthermore, impregnation itself results in a slight shift in this property.

Rise time (Figure 15) offers insights into the temporal evolution of AE signals. Matrix cracking, fiber-matrix debonding, and single-fiber breakage are associated with short rise times (typically under 100  $\mu$ s), corresponding to rapid stress release. In

contrast, delamination and fiber breakage from roving testing show considerably longer rise times, ranging from 300 to over 800  $\mu$ s. These may be associated with the progressive manner of the delamination and the sequential nature of fiber breakage inside a roving, which often appears as a fiber bundle failure. Rise time as a signal property may be helpful in the classification of damage mechanisms as well.

The average frequency distribution (Figure 16) clearly separates matrix or interface-dominated and fiber-dominated damage types. Matrix cracking, delamination, and fiber-matrix debonding occur in the lower frequency range (typically between 100–200 Hz), whereas fiber breakage consistently appears at higher frequencies, mainly up to 300 Hz.

Absolute energy (Figure 17) is a critical metric to distinguish low- and high-energy failure events. Delamination and matrix cracking display the lowest energy levels, reflecting matrix-related damage. In contrast, fiber-matrix debonding and fiber breakage exhibit higher energy values, with considerable variability and multiple outliers. These high-energy values indicate extensive and energetically intense damage mechanisms. The results indicate that absolute energy effectively separates the matrix-dominated matrix cracking and delamination from interface/fiber-related damage mechanisms.

Finally, signal strength (Figure 18) reflects the overall intensity of AE signals. Matrix cracking and delamination generate the weakest signals, aligning with their low energy and amplitude. Fiber-related

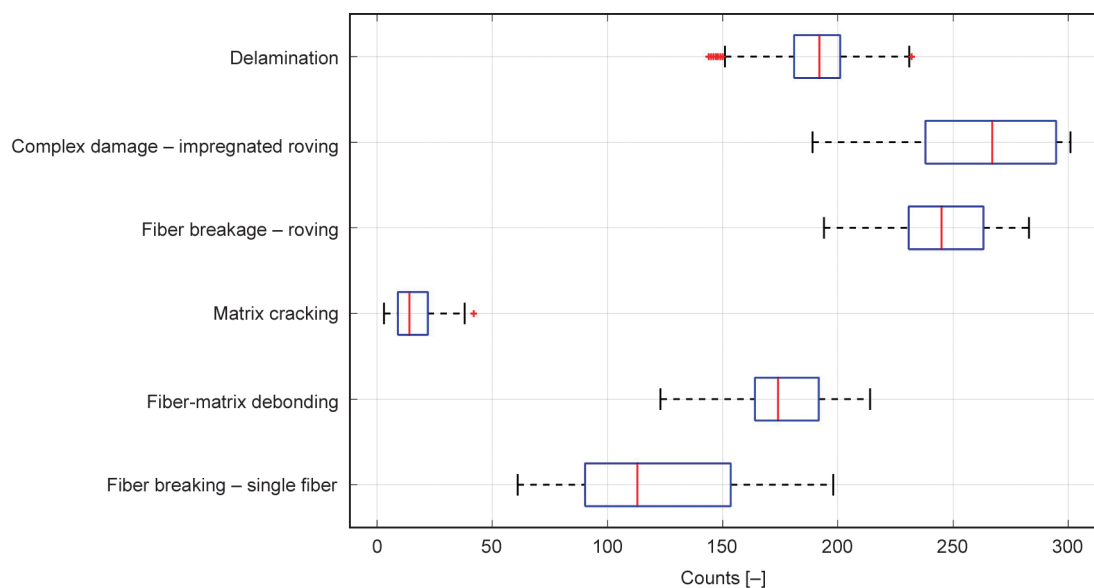


**Figure 14.** Counts distribution of various damage modes represented by horizontal box plots.

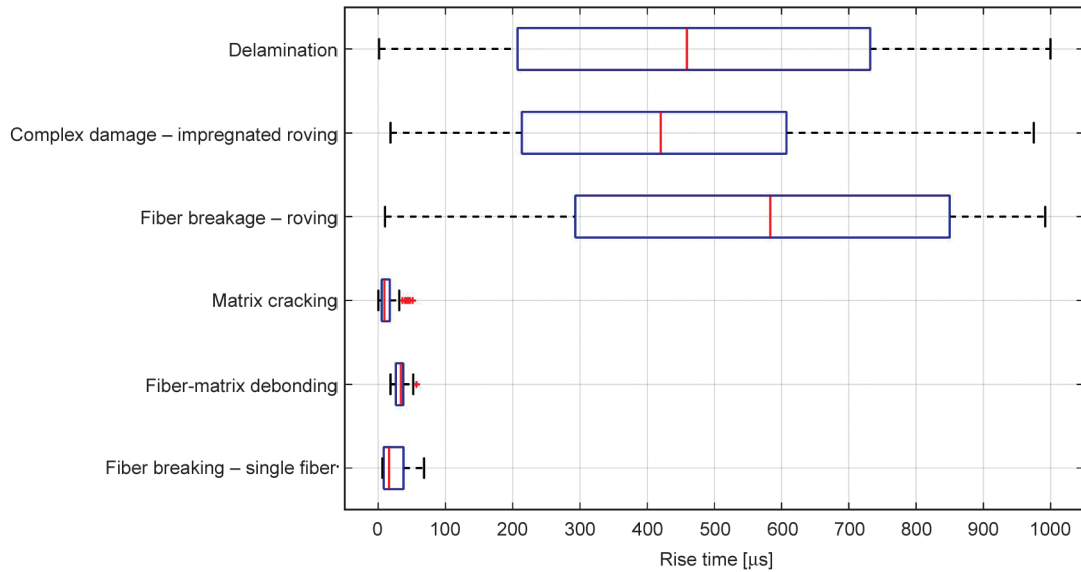


Figure 15. Rise time distribution of various damage modes represented by horizontal box plots.

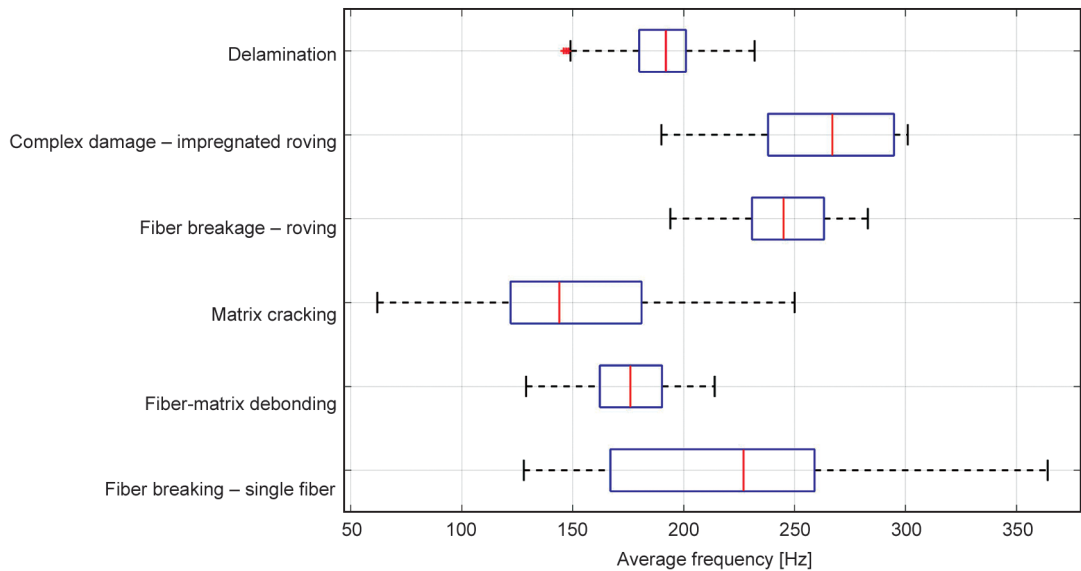


Figure 16. Average frequency distribution of various damage modes represented by horizontal box plots.

damage types, especially complex roving damage and fiber-matrix debonding, exhibit higher signal strengths. This parameter correlates strongly with absolute energy and supports the characterization of the severity of damage.

Due to the overlap in several cases in individual AE signal properties across damage mechanisms, relying on a single feature can often lead to misclassification. Therefore, a multidimensional approach involving several AE signal properties is required to improve the reliability of signal clustering. Figure 19 shows a simplified example of two-dimensional approach based on our results, demonstrating how combining amplitude and counts can already enhance class separability to some extent.

#### 4. Conclusions

We investigated the damage mechanisms of carbon fibre reinforced composites with epoxy matrix. We carried out specific tests that induce individual damage mechanisms. During the measurements, the signals emitted by the active damage mechanisms were acquired by the acoustic emission technique. Therefore, the conducted measurements provide information on the characteristic AE signals associated with the individual damage mechanisms. Tensile testing of the epoxy matrix was used to characterize matrix cracking, microbond tests were carried out to simulate fiber-matrix debonding, and short-beam shear tests were conducted to characterize delamination. Single fiber tensile and roving tensile testing results were

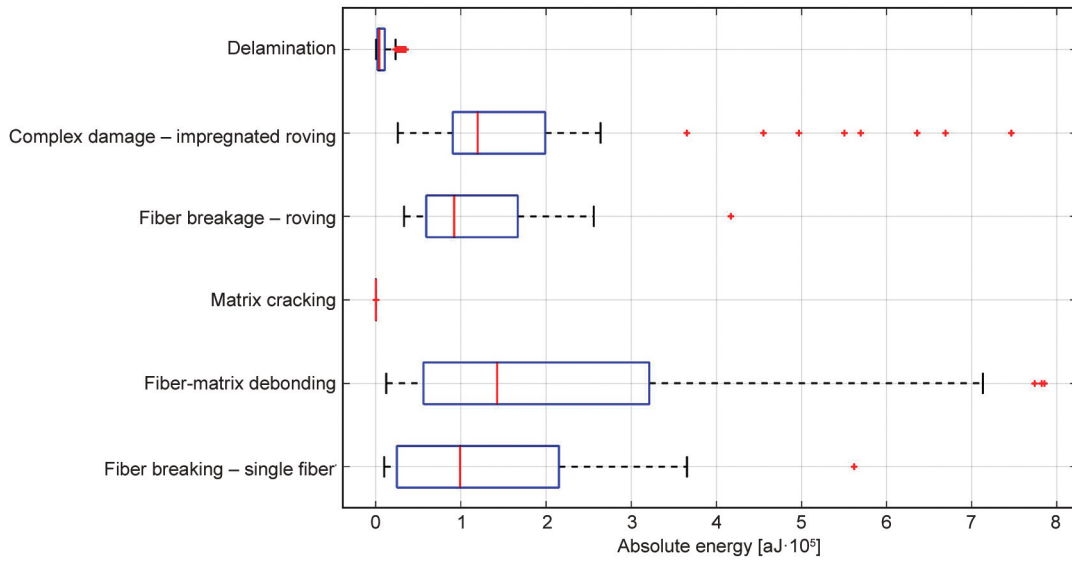


Figure 17. Absolute Energy distribution of various damage modes represented by horizontal box plots.

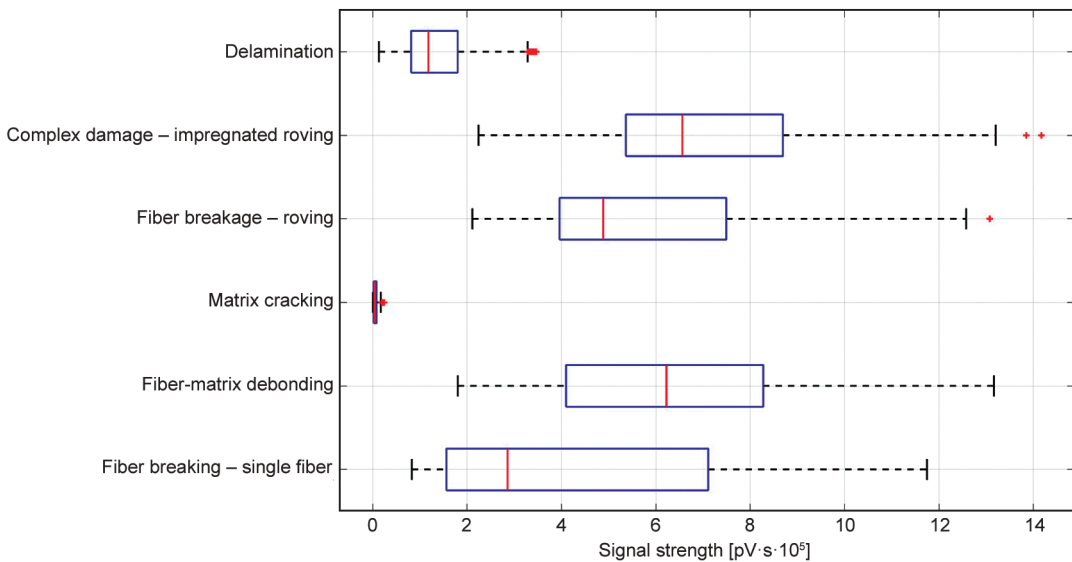


Figure 18. Signal strength distribution of various damage modes represented by horizontal box plots.

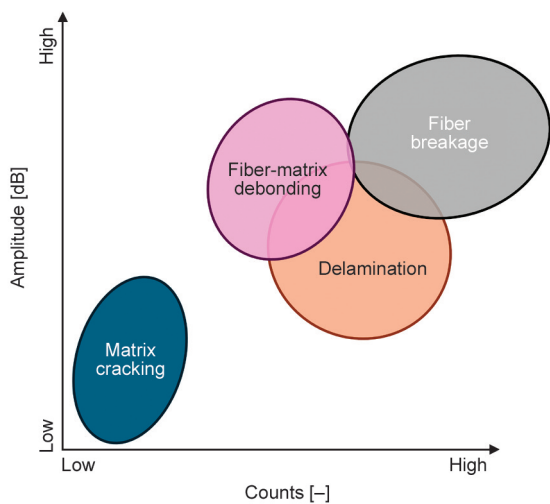


Figure 19. Illustration of two-dimensional classification based on our experimental results.

associated with fiber breakage. Furthermore, we investigated fiber breakage and fiber-matrix debonding by the tensile testing of impregnated rovings as well. The results indicate that each AE parameter contributes distinct information regarding identifying and analyzing the damage mechanisms in fiber-reinforced polymer composites. Although amplitude is especially valuable for differentiating various damage modes, it is not enough to create a reliable method for their identification. Therefore, a combined analysis of several AE parameters - amplitude, absolute energy, signal strength, counts, average frequency, and rise time - should be used to identify the damage modes and distinguish between them properly.

The experiments can provide a physical basis for classifying damage mechanisms in the composite

material based on AE data. Therefore, the results can be used for manual clustering or to support statistical clustering methods, where the specified characteristic signal property ranges can assist in preprocessing and labeling of AE data, and contribute to the physical validation of results. Furthermore, the results of this study may be used to create an artificial neural network (ANN) based system for the identification of damage modes.

## Acknowledgements

We would like to sincerely thank Dr. Gábor Romhány for his support in the AE experiments and evaluation. The research has been supported by the NRD Office (OTKA FK 142540). Gábor Szabó acknowledges the financial support received through the János Bolyai Scholarship of the Hungarian Academy of Sciences and ÚNKP-23-5-BME-415 New National Excellence Program.

Project no. 2022-2.1.1-NL-2022-00012 ‘National Laboratory for Cooperative Technologies’ has been implemented with the support provided by the Ministry of Culture and Innovation of Hungary from the National Research, Development and Innovation Fund, financed under the National Laboratories funding scheme. Project no. TKP-6-6/PALY-2021 has been implemented with the support provided by the Ministry of Culture and Innovation of Hungary from the National Research, Development and Innovation Fund, financed under the TKP2021-NVA funding scheme.

Project no. KDP-IKT-2023-900-I1-00000957/0000003 has been implemented with the support provided by the Ministry of Culture and Innovation of Hungary from the National Research, Development and Innovation Fund, financed under the KDP-2023 funding scheme. The project supported by the Doctoral Excellence Fellowship Programme (DCEP) is funded by the National Research Development and Innovation Fund of the Ministry of Culture and Innovation and the Budapest University of Technology and Economics. Special thanks to Vencel Bulman for his help with the experiments.

## References

- [1] Zhang J., Lin G., Vaidya U., Wang H.: Past, present and future prospective of global carbon fibre composite developments and applications. *Composites Part B: Engineering*, **250**, 110463 (2023).  
<https://doi.org/10.1016/j.compositesb.2022.110463>
- [2] Messaoud B., Amrane M. N.: Vibration analysis of damaged viscoelastic composite sandwich plate. *Periodica Polytechnica Mechanical Engineering*, **68**, 85–96 (2024).  
<https://doi.org/10.3311/PPme.19466>
- [3] Csvila P., Czigány T.: Multifunctional energy storage polymer composites: The role of nanoparticles in the performance of structural supercapacitors. *Express Polymer Letters*, **18**, 1023–1038 (2024).  
<https://doi.org/10.3144/expresspolymlett.2024.78>
- [4] Marton G. Zs., Szabó G.: Influencing the damage process and failure behaviour of polymer composites – A short review. *Express Polymer Letters*, **19**, 140–160 (2025).  
<https://doi.org/10.3144/expresspolymlett.2025.11>
- [5] Marton G. Z., Fendrik Á., Szabó G.: Manufacturing of composites with designed failure. *IOP Conference Series: Materials Science and Engineering*, **1313**, 012014 (2024).  
<https://doi.org/10.1088/1757-899X/1313/1/012014>
- [6] Magyar B., Czigany T., Szabó G.: Metal-alike polymer composites: The effect of inter-layer content on the pseudo-ductile behaviour of carbon fibre/epoxy resin materials. *Composites Science and Technology*, **215**, 109002 (2021).  
<https://doi.org/10.1016/j.compscitech.2021.109002>
- [7] Marino S. G., Czél G.: Improving the performance of pseudo-ductile hybrid composites by film-interleaving. *Composites Part A: Applied Science and Manufacturing*, **142**, 106233 (2021).  
<https://doi.org/10.1016/j.compositesa.2020.106233>
- [8] Alipour A., Lin R., Jayaraman K.: Enhancement of performance in flax/epoxy composites by developing interfacial adhesion using graphene oxide. *Express Polymer Letters*, **17**, 471–486 (2023).  
<https://doi.org/10.3144/expresspolymlett.2023.35>
- [9] Melaibari A., Wagih A., Basha M., Kabeel A. M., Lubineau G., Eltaher M. A.: Bio-inspired composite laminate design with improved out-of-plane strength and ductility. *Composites Part A: Applied Science and Manufacturing*, **144**, 106362 (2021).  
<https://doi.org/10.1016/j.compositesa.2021.106362>
- [10] Heslehurst R. B.: *Defects and damage in composite materials and structures*. CRC Press, Boca Raton (2014).
- [11] Zimmermann N., Wang P. H.: A review of failure modes and fracture analysis of aircraft composite materials. *Engineering Failure Analysis*, **115**, 104692 (2020).  
<https://doi.org/10.1016/j.engfailanal.2020.104692>
- [12] Talreja R., Singh C. V.: *Damage and failure of composite materials*. Cambridge University Press, Cambridge (2012).
- [13] Talreja R., Waas A. M.: Concepts and definitions related to mechanical behavior of fiber reinforced composite materials. *Composites Science and Technology*, **217**, 109081 (2022).  
<https://doi.org/10.1016/j.compscitech.2021.109081>
- [14] Hassani S., Mousavi M., Gandomi A. H.: Structural health monitoring in composite structures: A comprehensive review. *Sensors*, **22**, 153 (2022).  
<https://doi.org/10.3390/s22010153>
- [15] Saha N., Roy P., Topdar P.: Damage detection in composites using non-destructive testing aided by ANN technique: A review. *Journal of Thermoplastic Composite Materials*, **36**, 4997–5033 (2023).  
<https://doi.org/10.1177/08927057231172670>
- [16] Szabó G., Hliva V.: Detection of delamination in polymer composites by digital image correlation – Experimental test. *Polymers*, **11**, 523 (2019).  
<https://doi.org/10.3390/polym11030523>

- [17] Huang J., Wei Q., Zhuo L., Zhu J., Li C., Wang Z.: Detection and quantification of artificial delaminations in CFRP composites using ultrasonic thermography. *Infrared Physics and Technology*, **130**, 104579 (2023). <https://doi.org/10.1016/j.infrared.2023.104579>
- [18] Hliva V., Szebényi G.: Non-destructive evaluation and damage determination of fiber-reinforced composites by digital image correlation. *Journal of Nondestructive Evaluation*, **42**, 43 (2023). <https://doi.org/10.1007/s10921-023-00957-7>
- [19] Gao T., Wang Y., Qing X.: A new laser ultrasonic inspection method for the detection of multiple delamination defects. *Materials*, **14**, 2424 (2021). <https://doi.org/10.3390/ma14092424>
- [20] Livingston R., Koohbor B.: Characterizing fiber-matrix debond and fiber interaction mechanisms by full-field measurements. *Composites Part C: Open Access*, **7**, 100229 (2022). <https://doi.org/10.1016/j.jcomc.2022.100229>
- [21] Holmes J., Sommecal S., Das R., Stachurski Z., Compston P.: Digital image and volume correlation for deformation and damage characterisation of fibre-reinforced composites: A review. *Composite Structures*, **315**, 116994 (2023). <https://doi.org/10.1016/j.compstruct.2023.116994>
- [22] Wang B., Zhong S., Lee T-L., Fancey K. S., Mi J.: Non-destructive testing and evaluation of composite materials/structures: A state-of-the-art review. *Advances in Mechanical Engineering*, **12**, 1–28 (2020). <https://doi.org/10.1177/1687814020913761>
- [23] Jodhani J., Handa A., Gautam A., Ashwni, Rana R.: Ultrasonic non-destructive evaluation of composites: A review. *Materials Today: Proceedings*, **78**, 627–632 (2023). <https://doi.org/10.1016/j.matpr.2022.12.055>
- [24] Saeedifar M., Zarouchas D.: Damage characterization of laminated composites using acoustic emission: A review. *Composites Part B: Engineering*, **195**, 108039 (2020). <https://doi.org/10.1016/j.compositesb.2020.108039>
- [25] Barile C., Casavola C., Pappaletta G., Kannan V. P.: Damage monitoring of carbon fibre reinforced polymer composites using acoustic emission technique and deep learning. *Composite Structures*, **292**, 115629 (2022). <https://doi.org/10.1016/j.compstruct.2022.115629>
- [26] Khamedi R., Saeed A., Ghorbani A., Ghiami A., Erden S.: Damage characterization of carbon/epoxy composites using acoustic emission signals wavelet analysis. *Composite Interfaces*, **27**, 111–124 (2020). <https://doi.org/10.1080/09276440.2019.1601939>
- [27] Romhányi G., Czigány T., Karger-Kocsis J.: Failure assessment and evaluation of damage development and crack growth in polymer composites *via* localization of acoustic emission events: A review. *Polymer Reviews*, **57**, 397–439 (2017). <https://doi.org/10.1080/15583724.2017.1309663>
- [28] Karthik M. K., Kumar C. S.: A comprehensive review on damage characterization in polymer composite laminates using acoustic emission monitoring. *Russian Journal of Nondestructive Testing*, **58**, 705–721 (2022). <https://doi.org/10.1134/S106183092208006X>
- [29] Kalafat S., Sause M. G. R.: Acoustic emission source localization by artificial neural networks. *Structural Health Monitoring*, **14**, 633–647 (2015). <https://doi.org/10.1177/1475921715607408>
- [30] Oz F. E., Ahmadvashaghbash S., Ersoy N.: Damage mode identification in transverse crack tension specimens using acoustic emission and correlation with finite element progressive damage model. *Composites Part B: Engineering*, **165**, 84–95 (2019). <https://doi.org/10.1016/j.compositesb.2018.11.104>
- [31] Görbe Á., Marton G. Zs., Bárányi T.: Acoustic emission analysis of failure processes in polyethylene and recycled tire rubber blends. *Polymer Testing*, **147**, 108813 (2025). <https://doi.org/10.1016/j.polymertesting.2025.108813>
- [32] Ghadarah N., Ayre D.: A review on acoustic emission testing for structural health monitoring of polymer-based composites. *Sensors*, **23**, 6945 (2023). <https://doi.org/10.3390/s23156945>
- [33] de Groot P. J., Wijnen P. A. M., Janssen R. B. F.: Real-time frequency determination of acoustic emission for different fracture mechanisms in carbon/epoxy composites. *Composites Science and Technology*, **55**, 405–412 (1995). [https://doi.org/10.1016/0266-3538\(95\)00121-2](https://doi.org/10.1016/0266-3538(95)00121-2)
- [34] Gutkin R., Green C. J., Vangrattanachai S., Pinho S. T., Robinson P., Curtis P. T.: On acoustic emission for failure investigation in CFRP: Pattern recognition and peak frequency analyses. *Mechanical Systems and Signal Processing*, **25**, 1393–1407 (2011). <https://doi.org/10.1016/j.ymsp.2010.11.014>
- [35] Nikbakht M., Yousefi J., Hosseini-Toudeshky H., Minak G.: Delamination evaluation of composite laminates with different interface fiber orientations using acoustic emission features and micro visualization. *Composites Part B: Engineering*, **113**, 185–196 (2017). <https://doi.org/10.1016/j.compositesb.2016.11.047>
- [36] Rajendraboopathy S., Sasikumar T., Usha K. M., Vasudev E. S.: Artificial neural network a tool for predicting failure strength of composite tensile coupons using acoustic emission technique. *The International Journal of Advanced Manufacturing Technology*, **44**, 399–404 (2009). <https://doi.org/10.1007/s00170-008-1874-x>
- [37] Arumugam V., Shankar R. N., Sridhar B. T. N., Stanley A. J.: Ultimate strength prediction of carbon/epoxy tensile specimens from acoustic emission data. *Journal of Materials Science and Technology*, **26**, 725–729 (2010). [https://doi.org/10.1016/S1005-0302\(10\)60114-4](https://doi.org/10.1016/S1005-0302(10)60114-4)
- [38] Oz F. E., Ersoy N., Mehdikhani M., Lomov S. V.: Multi-instrument *in-situ* damage monitoring in quasi-isotropic CFRP laminates under tension. *Composite Structures*, **196**, 163–180 (2018). <https://doi.org/10.1016/j.compstruct.2018.05.006>
- [39] Sause M. G. R., Gribov A., Unwin A. R., Horn S.: Pattern recognition approach to identify natural clusters of acoustic emission signals. *Pattern Recognition Letters*, **33**, 17–23 (2012). <https://doi.org/10.1016/j.patrec.2011.09.018>